

Planar magnetic Paul traps for ferromagnetic particles

M. Perdriat , C. Pellet-Mary , T. Copie , and G. Hétet

Laboratoire de Physique de l'École Normale Supérieure, École Normale Supérieure, PSL Research University, CNRS, Sorbonne Université, Université Paris Cité, 24 rue Lhomond, 75231 Paris Cedex 05, France



(Received 21 December 2022; accepted 8 June 2023; published 28 September 2023)

We present a study on the trapping of hard ferromagnetic particles using alternating magnetic fields, with a focus on planar trap geometries. First, we realize and characterize a magnetic Paul trap design for millimeter-size magnets based on a rotating magnetic potential. Employing a physically rotating platform with two pairs of permanent magnets with opposite poles, we show stable trapping of hard ferromagnets a centimeter above the trap and demonstrate that the particle shape plays a critical role in the trapping. Finally, we propose a chip trap design that will open a path to studies of gyromagnetic effects with ferromagnetic microparticles.

DOI: [10.1103/PhysRevResearch.5.L032045](https://doi.org/10.1103/PhysRevResearch.5.L032045)

In the 1950s, Paul proposed to employ alternating electric fields to solve the conundrum imposed by Maxwell's equations [1] which prohibits levitation of charged particles using static electric fields. Although the electric field is zero on average, the slight particle displacement during one period of the electric field alternation can lead to an efficient dynamical stabilization of the particle. Since then, Paul traps have found countless applications such as in mass spectrometry and rf spectroscopy [2], ground state cooling of atoms [3], quantum computing [4], or more recently to quantum engineering of levitating particles [5,6]. Trapping magnets is also an important endeavor that has gained interest lately. A particularly intriguing direction is the search for atomiclike effects on magnet motion, stemming from the spin degree of freedom [7–9]. Observing such effects is under reach using trapped nanoferrromagnets or particles containing a large number of polarized spins and could lead to several applications in gyroscopy, magnetometry [10], spin mechanics [11,12], or in fundamental tests of quantum mechanics [13].

There exist several magnetic levitation protocols for ferromagnets. For instance, adding angular momentum to a magnet on top of a toroidal magnetic field can provide stable trapping. The mechanisms behind this so-called levitron were attributed to the combined action of the gyroscopic stability and the magnet's precession [14], both of which act to continuously align the magnet precession axis to the local magnetic field direction. Another widely used method is electromagnetic suspension (EMS) [15], which uses servo loops to counteract deviations of the particle motion away from a desired working point. A last example that shows efficient magnet levitation employs the diamagnetism of superconductors [12,16–18], with large reported mechanical quality factors [12,19] and foreseeably high control in the engineering of the magnet quantum motion.

Following the same logic as for charged particles, a trap that uses alternating magnetic fields may also offer strong harmonic confinement of magnets together with room-temperature operation. A major difference between magnetic Paul traps (MPTs) and electric Paul traps is that the magnetic energy depends on the ferromagnet orientation and thus the angular dynamics must be also controlled for stable levitation. A strong enough homogeneous magnetic field can nevertheless fix the direction of the magnet dipole moment without exerting any force on the magnet. The method was in fact already realized [20] shortly after having been employed for trapping neutral atoms in the early days of Bose-Einstein condensation [21]. The authors of Ref. [20] used a combination of permanent magnets and time varying currents in Helmholtz coils to enable ponderomotive confinement. Similar traps for large particles were then soon implemented [22–24]. In the present Letter, we demonstrate and characterize a magnetic Paul trap using alternating magnetic fields coming from physically rotating permanent magnets in a planar geometry. We then propose a planar on-chip design that will enable the trapping of micrometric particles, as well as enabling straightforward optical and inductive detection of their motion.

We start by showing the trapping of a ferromagnet for all six degrees of freedom, namely the three center-of-mass modes and the three librational modes, in a room-temperature tabletop setup. Instead of the stationary-wave geometry typically employed in electric Paul traps, here we use the running-wave version, where the field curvatures in the (x, y) plane rotate over time. We rotate magnetic fields using a physically rotating platform holding rigidly fixed permanent magnets to produce a ponderomotive potential in the (x, y) plane.

Figure 1(a) is a depiction of the platform that we employ. Opposite pairs of 5-mm-square magnets are oriented so that their magnetic moments point to the same direction. The magnets are glued on the periphery of a copper baseplate. The distance between the center of the opposite magnet pairs is 20 mm. The assembly is attached to the spinning arm of the motor from a mechanical chopper. The motor can make this system rotate at a maximum frequency of 100 Hz, thus

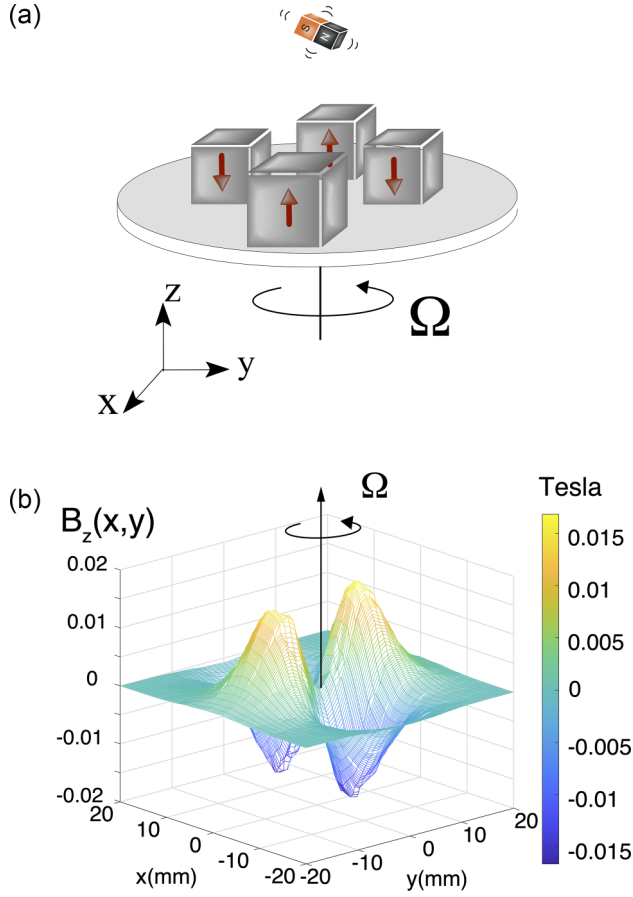


FIG. 1. (a) Sketch of the magnetic Paul trap. (b) Numerical simulations showing the projection of the magnetic field vector on the z axis as a function of x and y , at a distance $z = 1$ cm from the trap.

generating fast rotating magnetic fields along the x, y directions. The z direction can also be confined when the particle shape is taken into account, as will be explained later.

Consider a particle of mass m which can move in a plane subjected to a saddle potential rotating at the frequency $\Omega/2\pi$. We designate by (x, y) the spatial coordinate of the particle in the laboratory-fixed frame and (X, Y) the coordinate in the rotating saddle frame. Adding an extra homogeneous magnetic field along z fixes the particle angle along the z direction. As shown in the Supplemental Material (SM) [25], because of the typically large moment of inertia of the particles we trap, only a moderate homogeneous B field (in the mT range) is enough to ensure that the particle magnetic moment direction is not being defined by the B fields from the rotating magnets.

Figure 1(b) is the result of numerical simulations of the static magnetic field component along the z direction as a function of x and y at a distance $z = 1$ cm from the four-magnet trap. The magnetic field reaches about 0.1 T at maximum, and features a hyperbolic paraboloid shape close to $(x, y) = (0, 0)$. In the rotating frame, the magnetic field projection along z around the saddle point reads

$$B_z(X, Y) = \frac{1}{2}B_z''(z)(X^2 - Y^2), \quad (1)$$

where $B_z''(z)$ is the curvature of the magnetic field component along z . In this frame, two forces must be added: the centrifugal force $\mathbf{F}_{\text{cen}} = m\Omega^2(X\mathbf{e}_X + Y\mathbf{e}_Y)$ and the Coriolis force $\mathbf{F}_{\text{Cor}} = -2m(\Omega\mathbf{e}_Z) \times (\dot{X}\mathbf{e}_X + \dot{Y}\mathbf{e}_Y)$. The confinement along x and y comes from the competition between \mathbf{F}_{cen} and \mathbf{F}_{Cor} . In the laboratory-fixed frame, the magnetic field is time dependent and reads

$$B_z(\mathbf{r}, t) = \frac{B_z''(z)}{2}[(x^2 - y^2) \cos(2\Omega t) - 2xy \sin(2\Omega t)]. \quad (2)$$

The coupled set of equations of motions for the center-of-mass coordinates subjected to $B_z(\mathbf{r}, t)$ can be solved straightforwardly by averaging over one period of the trap oscillation (see Sec. I in SM [25]). This procedure leads to ponderomotive confinements both in the x and y directions at trapping frequencies that are given by

$$\frac{\omega_{x,y}}{2\pi} = \frac{B_{\text{sat}}|B_z''(z)|}{\mu_0\pi\rho_m\Omega}. \quad (3)$$

Here, ρ_m is the magnet density and $B_{\text{sat}} \approx 1$ T is the magnetization at saturation of the magnet. Using $\Omega/2\pi \approx 100$ Hz, we obtain $\frac{\omega_{x,y}}{2\pi}$ in the Hz range when the magnet lies a centimeter above the trap. Notably, in this geometry, the magnetic field is zero at the center $(x, y) = (0, 0)$ at any position along z . If the particle was a pointlike magnet, there would be no confinement in the z direction. A homogeneously magnetized particle whose form is invariant by $\pi/2$ rotations about an axis \mathbf{e}_s , will also not experience any force along z if the symmetry axis \mathbf{e}_s coincides with \mathbf{e}_z . Indeed, the total force exerted by the four magnets on the whole body cancels out at any point in time. However, any deviation of the particle symmetry axis from the z direction imposed by the external homogeneous magnetic field may give rise to a net force along z onto the particle. When averaged over a cycle of the trap rotation, the particle would feel a ponderomotive force that pushes it away from the $z = 0$ point. Taking a parallelepiped with magnetic moment along z , with a length l along x and a square cross section with a side length $h < l$, one finds (see Sec. II in SM [25]) that the time-dependent potential along the z direction reads

$$E_{\text{mag}}(\mathbf{r}, t) \approx \frac{1}{2}m\omega_z^2 \cos(2\omega t)z^2, \quad (4)$$

where

$$\omega_z = \sqrt{\frac{B_{\text{sat}}a_2}{12\mu_0\rho_m}(l^2 - h^2)}. \quad (5)$$

Note that the radial potential is not impacted by this shape effect to first order. As expected, the force is proportional to $a_2 = \partial^2 B_z''(z)/\partial z^2$ and the decrease of the magnetic curvature $B_z''(z)$ along z gives rise to an outward force when averaged over one oscillation period. There will, in turn, be a local energy minimum owing to gravity, thus confining the particle at a distance $d \approx 1$ cm from the trap (see Sec. I in SM [25]).

Experimentally, we find that at frequencies $\Omega/2\pi$ in the 50–100 Hz range, millimeter-scale magnets can stably levitate for extended periods of time (more than hours) at a distance

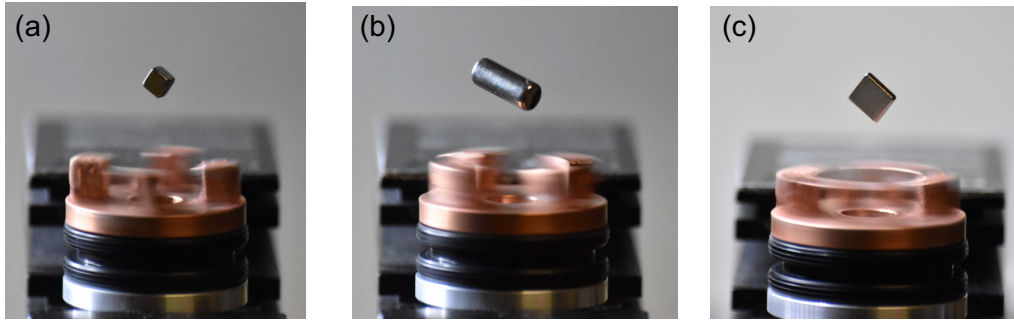


FIG. 2. Photographs showing three magnets levitating above the rotating magnetic saddle: (a) a 3-mm cube, (b) a 10-mm-long cylinder with a 5 mm diameter, and (c) a parallelepiped with a short side length of 1 mm and a 5 mm \times 5 mm flat square magnet. In these experiments, the magnets do not rotate over time in any direction (see the movie in the SM [25]).

$d \approx 15$ mm from the rotating baseplate where magnets are glued. Figures 2(a)–2(c) show three photos of levitating magnets of different shapes and sizes. All three are neodymium iron boron magnets with a nickel coating. The three magnets are perfectly stable for all six degrees of freedom and over extended periods of time. A video of a levitating magnet can also be found in the Supplemental Material [25]. We found that placing magnets in a small water container above the trap and then removing the water using a syringe once they are stably trapped ensures efficient loading. The ease with which we can trap under water most likely stems from the increased capture volume as the damping is increased. After optimizing external homogeneous magnetic field directions and amplitudes using an extra permanent magnet, all of these magnets can be made stable angularly. The homogeneous magnetic field can indeed change the orientation of the magnet without perturbing the particle center of mass, as long as the magnetic field gradients at the particle location are negligible compared to the effective time-averaged magnetic field gradients from the saddle. We also found that the stator of the motor itself generates a strong enough static magnetic field that can also orient the magnet.

Numerical simulations (see Sec. I B in SM [25]) show good agreement with the experimental observations. In particular, the observed trapping height agrees with a model taking into account the particle shape. We also found further evidence that confinement along the z direction arises because of the particle shape by performing experiments with a millimeter-size spherical magnet. Confinement along z was not observed for such particles, in agreement with Eq. (5), which predicts no confinement if $l \approx h$ in the trap center. Note that this formula is only valid for small enough particles (see Sec. I B in SM [25] for a description of the limits of the model). To ensure confinement in the transverse plane while measuring the z -dependent force on this spherical particle, we enclose it in a small glass tube and read out its z motion as the tube is displaced transversally. Figure 3(b) shows a picture of the setup and Fig. 3(a) is a schematic showing the employed parametrization. Figure 3(c) shows the data where the center-of-mass position z is monitored as a function of x . The particle experiences no outward force when the tube is positioned such that $|x| < 2.5$ mm and remains at the bottom of the tube. As the tube is displaced, the particle is lifted up, with a maximum height at $|x| \approx 19$ mm, and then falls

down again. This behavior is very well captured by numerical simulations where the outward force comes from the competition between ponderomotive force and gravity. Note also that, although extensive tests have been made, no trapping could be obtained after rotating the whole apparatus upside down, which shows that the z confinement is not solely due to the rotating magnetic field and that gravity plays a role. One last check is the dependency of the particle position with $\Omega/2\pi$. Figure 3(d) shows the height z of a trapped 2.5-mm-side cubic magnet (Fig. 2), as a function of $\Omega/2\pi$. z is seen to decrease as the trap rotation frequency is increased, as expected from the ponderomotive nature of the outward force competing with gravity.

The off-centered position of the particle along z is very convenient for the large optical access required for optical readout of the motion. It will also facilitate the particle levitation in a vacuum chamber without having to integrate the rotating platform. As is the case with magnetic traps for neutral atoms or with ion traps, the most versatile way to trap particles while reaching high trapping frequencies together with open access is to employ chip-based designs consisting of current-carrying wires. Here, we propose the planar trap design depicted in Fig. 4(a) where an alternating current $i_1(t)$ runs through a microwire in an externally applied homogeneous field $\mathbf{B}_0 = B_0 \mathbf{e}_z$. The total applied magnetic field $\mathbf{B}_{\text{tot}}(\mathbf{r}, t)$ on the ferromagnet at the center of this ring is the sum of a homogeneous field \mathbf{B}_0 and an oscillating parabolic magnetic field $\mathbf{B}_1(\mathbf{r}, t)$ which reads

$$\mathbf{B}_1(\mathbf{r}, t) = \frac{B_1''}{2} \left[\left(z^2 - \frac{1}{2}(x^2 + y^2) \right) \mathbf{e}_z - (xz\mathbf{e}_x + yz\mathbf{e}_y) \right] \cos(\Omega t), \quad (6)$$

where $(\mathbf{e}_x, \mathbf{e}_y, \mathbf{e}_z)$ is the laboratory-fixed axis, (x, y, z) are spatial coordinates, B_1'' is the curvature of $\mathbf{B}_1(\mathbf{r}, t)$, and $\Omega/2\pi$ is the frequency of the magnetic field oscillation.

We consider a hard ferromagnetic neodymium microsphere with a radius $a = 1$ μm . We use the zyz convention for the three Euler angles (α, β, γ) that parametrize the orientation of the magnet as well as the body-fixed magnetic moment orientation $\boldsymbol{\mu}$ (see Sec. II in SM [25]). The norm of the magnetic moment is $\mu = B_{\text{sat}}V/\mu_0$, where V the volume of the ferromagnet and $B_{\text{sat}} \approx 1.0$ T is the magnetization at saturation.

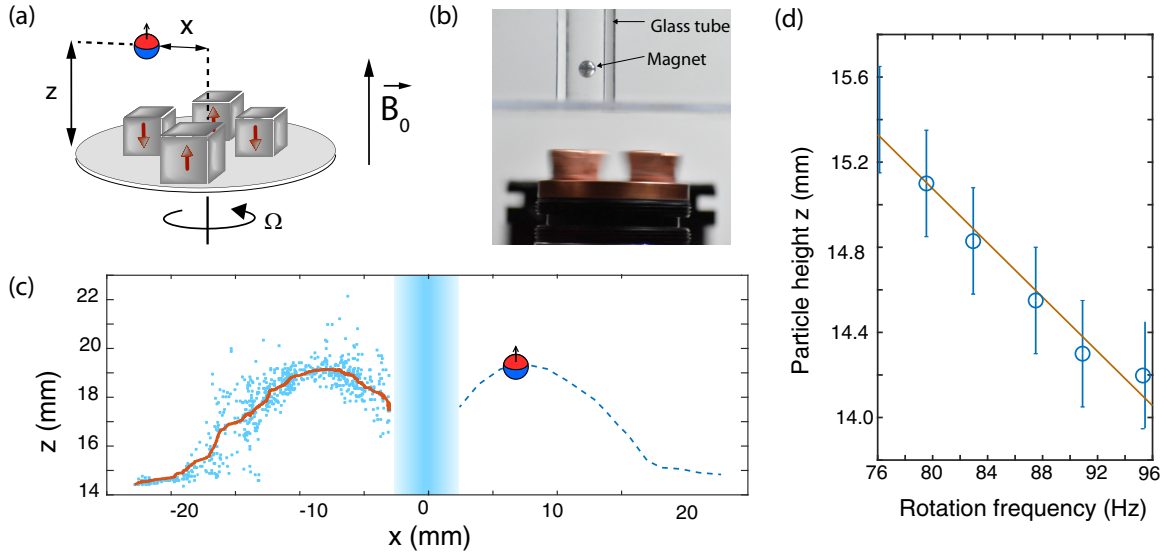


FIG. 3. (a) Schematic showing the parametrization of the particle coordinates. (b) Picture of the setup showing the glass tube where the particle is enclosed. (c) Measured position of the center of mass of a spherical 1-mm-diameter magnet as a function of the distance from the platform rotation axis. The central blue area indicates the range of x values where the particle sits at the bottom of the glass tube. (d) Position of the center of mass of a square magnet along z as a function of the rotation frequency $\Omega/2\pi$.

In the (x, y, z) basis, the magnetic moment is expressed as

$$\begin{aligned} \boldsymbol{\mu} = & -\mu(-c_\alpha s_{\tilde{\beta}} c_\gamma - s_\alpha s_\gamma) \mathbf{e}_x \\ & -\mu(c_\alpha s_\gamma - s_\alpha s_{\tilde{\beta}} c_\gamma) \mathbf{e}_y - \mu c_{\tilde{\beta}} c_\gamma \mathbf{e}_z, \end{aligned} \quad (7)$$

where c_i and s_i designate the cosine and sine function with arguments i and $\tilde{\beta}$ is the shifted nutation angle defined as $\tilde{\beta} = \beta - \pi/2$. By performing a second-order Taylor expansion of the microsphere magnetic energy $E_{\text{mag}} = -\boldsymbol{\mu} \cdot \mathbf{B}_{\text{tot}}(\mathbf{r}, t)$ around the position $(\tilde{\beta}, \gamma, x, y, z) = 0$, we obtain

$$\begin{aligned} E_{\text{mag}} = & \mu B_0 \left(\frac{\gamma^2}{2} + \frac{\tilde{\beta}^2}{2} \right) \\ & - \frac{\mu B_1''}{2} \left(z^2 - \frac{1}{2}(x^2 + y^2) \right) \cos(\Omega t). \end{aligned} \quad (8)$$

Within the stability conditions (see Sec. I B in SM [25]), the alternating magnetic potential leads to a pseudoharmonic confinement of the center-of-mass modes. After averaging the potential over one period of the magnetic field oscillation, we obtain the secular frequencies

$$\omega_\gamma = \omega_{\tilde{\beta}} = \sqrt{\frac{5}{2} \frac{B_0 B_{\text{sat}}}{\mu_0 \rho_m a^2}} \quad (9)$$

and

$$\tilde{\omega}_z = 2\tilde{\omega}_x = 2\tilde{\omega}_y = \frac{\Omega}{2} \frac{|q_z|}{\sqrt{2}}, \quad (10)$$

where $q_z = -2q_x = -2q_y = 2B_1'' B_{\text{sat}} / (\mu_0 \rho_m \Omega^2)$. Taking $q_z = 0.2$, where the secular harmonic approximation is valid and the following experimentally accessible values, $B_0 = 10$ mT, $B_1'' = 10^5$ T m $^{-2}$, and $\Omega = (2\pi)2.0$ kHz, we obtain $\omega_\gamma = \omega_{\tilde{\beta}} = (2\pi)300$ kHz and $\tilde{\omega}_z = 2\tilde{\omega}_x = 2\tilde{\omega}_y =$

$(2\pi)100$ Hz. These trapping frequencies are on the order of the trapping frequencies that can be achieved using superconducting traps for micromagnets [12,19], albeit here using a room-temperature setup. Figure 4(b) shows the result of numerical simulations where the center-of-mass motion for the x (blue curve) and z (red curve) modes evolve as a function of time for a Paul trap frequency $\Omega/2\pi = 1.7$ kHz. We see that as the magnet is displaced away from the position $x, z = 0$, a small high-frequency oscillation appears after which the particle is brought back to $x, z = 0$. This observation is in accordance with the expected principle of the ponderomotive confinement and in good agreement with the above analytical calculations.

The shift of the center-of-mass position induced by gravity is $z_0 = -g/\tilde{\omega}_z^2 \approx -20$ μm . Such a shift will generate micromotion in the \mathbf{e}_z direction as well as a small coupling between the center of mass and the angular modes. We found that the gravity can however be compensated for by an external electric field if the particle is electrically charged or using a magnetic field gradient generated by a current $i_2(t)$ such that $\mathbf{B}_2 = B_2'(z\mathbf{e}_z - x/2\mathbf{e}_x - y/2\mathbf{e}_y)$ with $B_2' = mg/\mu = 8.0 \times 10^{-2}$ T m $^{-1}$. The coupling between the center of mass and the angular modes induced by this extra field can safely be neglected here (see Sec. II in SM [25]).

While it is straightforward to experimentally generate the magnetic field \mathbf{B}_0 , the generation of an oscillating magnetic field with a curvature $B_1'' = 10^5$ T m $^{-2}$ requires a carefully engineered trap. We propose to employ a high-purity gold double-loop microtrap with radii $r_1 = 100$ μm and $r_2 = 200$ μm made by lithography, on a silicon chip with alternating currents $i_k(t) = i_k \cos(\omega t)$, $k = \{1, 2\}$ with $-2i_1 = i_2$. The condition $i_1/i_2 = -r_1/r_2$ further suppresses the magnetic field at $\mathbf{r} = \mathbf{0}$ while keeping its harmonic dependency. The magnetic field curvature reads $B_1'' = -\frac{9}{16}\mu_0 i_1/r_1^3$. This type of microchip can carry current of 10^5 A/cm 2 without

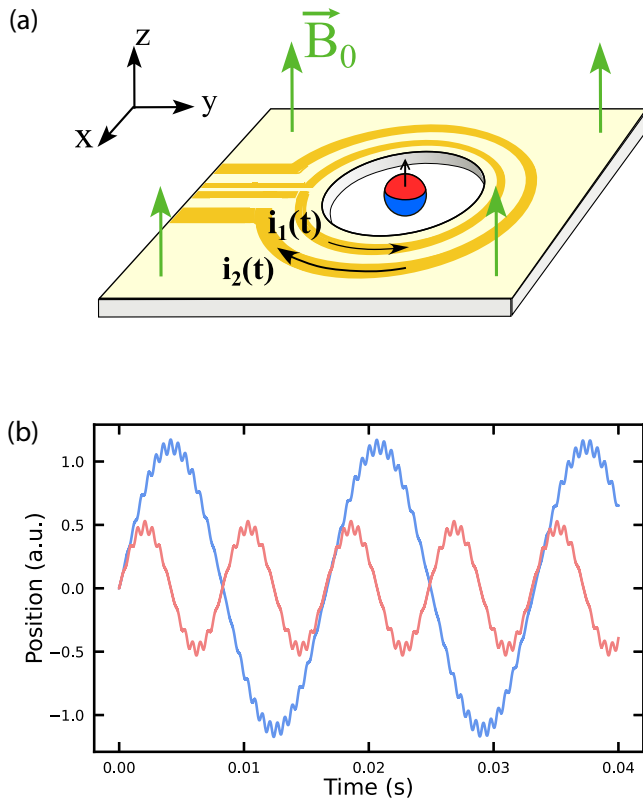


FIG. 4. (a) Depiction of the current-carrying trap design. (b) Simulations showing the center-of-mass motion in the x direction (blue curve) and the z direction (red curve) for a trapping frequency $\Omega/2\pi = 1.7$ kHz, an initial position $x_0 = 0$, $z_0 = 0$, and an initial velocity $\dot{x}_0 \neq 0$, $\dot{z}_0 \neq 0$.

experiencing too much heating [28,29]. With a 50- μm -large and 2- μm -thin gold layer, the current i_1 equals 0.1 A which leads to the desired value $B_1'' \approx 10^5 \text{ T m}^{-2}$. The induced currents generated by one loop onto the other are found to be negligible (see Sec. III in SM [25]). The eddy currents created inside the levitating ferromagnet are also negligible compared to the gas dissipation process even under high vacuum (see Sec. III in SM [25]). We thus expect no heating of the particle in this parameter regime.

The ability to control translational and rotational degrees of freedom of trapped particles with high precision has led to new opportunities for fundamental and applied research [6]. The high sensitivities of levitated objects to forces and torques in the motional ground state motivates research on tests of spin-mechanical coupling in the mesoscopic regime where gyromagnetic effects play a role. It is arguably beneficial to enrich the set of tools available to release some constraints that may be present in some trapping systems. As an example, optical levitation is typically prone to particle heating [30–32] and trapped charged particles do not lend themselves easily to approaching objects such as microfabricated optical components or other two-level systems [11] at distances below the micron. The presented magnetic Paul trap seems not to suffer from these problems and will thus enrich this already multidisciplinary research field.

We are thankful for fruitful discussions with R. Folman, D. Budker, J. Wei, R. Blatt, O. Romero-Isart, and P. Huillery. G.H. acknowledges funding from the Ile-de-France region in the framework of the DIM SIRTEQ. This project was funded within the QuantERA II Programme that has received funding from the European Union's Horizon 2020 research and innovation programme under Grant Agreement No. 101017733.

- [1] W. Paul, Electromagnetic traps for charged and neutral particles, *Rev. Mod. Phys.* **62**, 531 (1990).
- [2] M. Welling, H. Schuessler, R. Thompson, and H. Walther, Ion/molecule reactions, mass spectrometry and optical spectroscopy in a linear ion trap, *Int. J. Mass Spectrom. Ion Processes* **172**, 95 (1998).
- [3] C. Monroe, D. M. Meekhof, B. E. King, S. R. Jefferts, W. M. Itano, D. J. Wineland, and P. Gould, Resolved-Sideband Raman Cooling of a Bound Atom to the 3D Zero-Point Energy, *Phys. Rev. Lett.* **75**, 4011 (1995).
- [4] J. I. Cirac and P. Zoller, Quantum Computations with Cold Trapped Ions, *Phys. Rev. Lett.* **74**, 4091 (1995).
- [5] M. Perdriat, C. Pellet-Mary, P. Huillery, L. Rondin, and G. Hétet, Spin-mechanics with nitrogen-vacancy centers and trapped particles, *Micromachines* **12**, 651 (2021).
- [6] C. Gonzalez-Ballester, M. Aspelmeyer, L. Novotny, R. Quidant, and O. Romero-Isart, Levitodynamics: Levitation and control of microscopic objects in vacuum, *Science* **374**, eabg3027 (2021).
- [7] D. F. Jackson Kimball, A. O. Sushkov, and D. Budker, Precessing Ferromagnetic Needle Magnetometer, *Phys. Rev. Lett.* **116**, 190801 (2016).
- [8] C. C. Rusconi, V. Pöschhacker, K. Kustura, J. I. Cirac, and O. Romero-Isart, Quantum Spin Stabilized Magnetic Levitation, *Phys. Rev. Lett.* **119**, 167202 (2017).
- [9] K. Kustura, V. Wachter, A. E. Rubio López, and C. C. Rusconi, Stability of a magnetically levitated nanomagnet in vacuum: Effects of gas and magnetization damping, *Phys. Rev. B* **105**, 174439 (2022).
- [10] A. Vinante, C. Timberlake, D. Budker, D. F. Jackson Kimball, A. O. Sushkov, and H. Ulbricht, Surpassing the Energy Resolution Limit with Ferromagnetic Torque Sensors, *Phys. Rev. Lett.* **127**, 070801 (2021).
- [11] P. Huillery, T. Delord, L. Nicolas, M. Van Den Bossche, M. Perdriat, and G. Hétet, Spin mechanics with levitating ferromagnetic particles, *Phys. Rev. B* **101**, 134415 (2020).
- [12] J. Gieseler, A. Kabcenell, E. Rosenfeld, J. D. Schaefer, A. Safira, M. J. A. Schuetz, C. Gonzalez-Ballester, C. C. Rusconi, O. Romero-Isart, and M. D. Lukin, Single-Spin Magnetomechanics with Levitated Micromagnets, *Phys. Rev. Lett.* **124**, 163604 (2020).
- [13] C. Timberlake, A. Vinante, F. Shankar, A. Lapi, and H. Ulbricht, Probing modified gravity with magnetically levitated resonators, *Phys. Rev. D* **104**, L101101 (2021).

- [14] M. D. Simon, L. O. Heflinger, and S. L. Ridgway, Spin stabilized magnetic levitation, *Am. J. Phys.* **65**, 286 (1997).
- [15] E. Bachelet, Levitating transmitting apparatus, U.S. Patent No. 1020943A (1911).
- [16] J. Druge, C. Jean, O. Laurent, M.-A. Méasson, and I. Favero, Damping and non-linearity of a levitating magnet in rotation above a superconductor, *New J. Phys.* **16**, 075011 (2014).
- [17] V. Nemoskalenko, E. Brandt, A. Kordyuk, and B. Nikitin, Dynamics of a permanent magnet levitating above a high- T_c superconductor, *Physica C: Supercond.* **170**, 481 (1990).
- [18] J. R. Hull and A. Cansiz, Vertical and lateral forces between a permanent magnet and a high-temperature superconductor, *J. Appl. Phys.* **86**, 6396 (1999).
- [19] A. Vinante, P. Falferi, G. Gasbarri, A. Setter, C. Timberlake, and H. Ulbricht, Ultralow Mechanical Damping with Meissner-Levitated Ferromagnetic Microparticles, *Phys. Rev. Appl.* **13**, 064027 (2020).
- [20] C. Sackett, E. Cornell, C. Monroe, and C. Wieman, A magnetic suspension system for atoms and bar magnets, *Am. J. Phys.* **61**, 304 (1993).
- [21] E. A. Cornell, C. Monroe, and C. E. Wieman, Multiply Loaded, ac Magnetic Trap for Neutral Atoms, *Phys. Rev. Lett.* **67**, 2439 (1991).
- [22] R. Bassani, Stability of permanent magnet bearings under parametric excitations, *Tribol. Trans.* **48**, 457 (2005).
- [23] R. Bassani, A stability space of a magnetomechanical bearing, *J. Dyn. Syst., Meas., Control* **129**, 178 (2007).
- [24] R. Bassani, Dynamic stability of passive magnetic bearings, *Nonlinear Dyn.* **50**, 161 (2007).
- [25] See Supplemental Material at <http://link.aps.org/supplemental/10.1103/PhysRevResearch.5.L032045> for a detailed theoretical treatment of the magnet stability and a video of a trapped magnet, which includes Refs. [26,27].
- [26] O. Kirillov and M. Levi, M. A Coriolis force in an inertial frame, *Nonlinearity* **30**, 1109 (2017).
- [27] H. Dehmelt, Radiofrequency spectroscopy of stored ions I: Storage, *Adv. At. Mol. Phys.* **3**, 53 (1968).
- [28] R. Folman, P. Krüger, D. Cassetari, B. Hessmo, T. Maier, and J. Schmiedmayer, Controlling Cold Atoms using Nanofabricated Surfaces: Atom Chips, *Phys. Rev. Lett.* **84**, 4749 (2000).
- [29] L. Feenstra, L. M. Andersson, and J. Schmiedmayer, Microtraps and atom chips: Toolboxes for cold atom physics, *Gen. Relativ. Gravit.* **36**, 2317 (2004).
- [30] A. T. M. A. Rahman, A. C. Frangskou, M. S. Kim, S. Bose, G. W. Morley, and P. F. Barker, Burning and graphitization of optically levitated nanodiamonds in vacuum, *Sci. Rep.* **6**, 21633 (2016).
- [31] L. P. Neukirch, J. Gieseler, R. Quidant, L. Novotny, and A. N. Vamivakas, Observation of nitrogen vacancy photoluminescence from an optically levitated nanodiamond, *Opt. Lett.* **38**, 2976 (2013).
- [32] T. M. Hoang, J. Ahn, J. Bang, and T. Li, Electron spin control of optically levitated nanodiamonds in vacuum, *Nat. Commun.* **7**, 12250 (2016).